Chapter 3

Spectral Efficiency Analysis of Filter Bank Multi-Carrier (FBMC)-Based 5G Networks with Estimated Channel State Information (CSI)

Haijian Zhang, Hengwei Lv and Pandong Li

Additional information is available at the end of the chapter

http://dx.doi.org/10.5772/66057

Abstract

Filter bank multi-carrier (FBMC) modulation, as a potential candidate for physical data communication in the fifth generation (5G) wireless networks, has been widely investigated. This chapter focuses on the spectral efficiency analysis of FBMC-based cognitive radio (CR) systems, and spectral efficiency comparison is conducted with another three types of multi-carrier modulations: orthogonal frequency division multiplexing (OFDM), generalized frequency division multiplexing (GFDM), and universal-filtered multi-carrier (UFMC). In order to well evaluate and compare the spectral efficiency, we propose two resource allocation (RA) algorithms for single-cell and two-cell CR systems, respectively. In the single-cell system, the RA algorithm is divided into two sequential steps, which incorporate subcarrier assignment and power allocation. In the two-cell system, a noncooperative game is formulated and the multiple access channel (MAC) technique assists to solve the RA problem. The channel state information (CSI) between CR users and licensed users cannot be precisely known in practice, and thus, an estimated CSI is considered by defining a prescribed outage probability of licensed systems. Numerical results show that FBMC can achieve the highest channel capacity compared with another three waveforms.

Keywords: filter bank multi-carrier, spectral efficiency, resource allocation, cognitive radio, 5G networks

1. Introduction

With the increasing demand of communication quality, the fifth generation (5G) communication networks have shown development needs of high speed, low latency, high spectrum

efficiency, etc. [1]. As a result, people anticipate that the final outcome for 5G waveforms may include an adaptive solution, which means using the optimum waveform for any given situation. Nowadays, one key element of the cellular communication system is the multiple access technology that is used. Thus, the multi-carrier modulation (MCM) has been a research hotspot of the communication field due to its ability of suppressing the inter-symbol interference (ISI) and inter-channel interference (ICI). The orthogonal frequency division multiplexing (OFDM) is a typical style of MCM, which has been used in the fourth generation (4G) communication systems [2]. Although OFDM has many advantages, it still cannot satisfy the requirements of 5G networks [1]. With the higher level of processing that will be available, new 5G waveforms are being considered and evaluated for using with the new system. There have been some other MCM waveforms studied by the scholars around the world, including the well-known modulation schemes: filter bank multi-carrier (FBMC), generalized frequency division multiplexing (GFDM), and universal-filtered multi-carrier (UFMC) [3]. Each of them has its own advantages and disadvantages [4]. The modulation schemes used for the future 5G networks should have a significant impact on the whole performance and will play a major role in determining the performance and complexity of communication systems; however, single technique is not likely to meet all the requirements. In order to drive 5G standardization, academia is engaging in various collaborative projects such as METIS [5] and 5GNOW [6]. The purpose is to guarantee that the 5G can achieve commercialization in 2020.

In the future 5G networks, there needs more frequency resource for better communication. This requirement becomes particularly important because we have been facing the problem of frequency scarcity. However, in traditional spectrum management policy, there are a large amount of frequency bands which are not sufficiently utilized in most of the time. This results in a serious conflict between the target for better communication and the fact for spectrum scarcity. Cognitive radio (CR) [7–9] and FBMC [10–16] techniques, which are capable of efficiently exploiting the spectrum hole, can be considered to apply in 5G networks. CR technology is considered to be one of the most important technologies to improve the spectral efficiency. It can utilize the flexible and complex algorithms to control the interference to primary users (PUs). By adopting adaptive software, the CR devices are able to reconfigure their communication functions to the requirements of secondary users (SUs), while FBMC has a negligible frequency spectrum leakage, which has high robustness to the interference resulting from frequency offset. Therefore, it does not need to set the guard band in frequency domain, which greatly improves the spectral efficiency. In addition, FBMC can flexibly control the interference between adjacent subcarriers, which are unsynchronized. These advantages make FBMC more and more popular in the academic field. In recent years, the scholars have studied the FBMC system in terms of the spectral efficiency analysis [17], system complexity analysis [18], prototype filter design [19–21], frequency offset estimation [22], multiple-input multiple-output (MIMO) [23], and so on.

This chapter mainly analyses the spectral efficiency of FBMC in the context of CR systems. The results of other MCM waveforms give a better characterization of performance comparison to FBMC. In order to clarify the desirable property of FBMC, two different network scenarios

http://dx.doi.org/10.5772/66057

including single cell and two cells are taken into consideration. Specifically, for single-cell systems, we solve the uplink resource allocation (RA) problem by two sequential steps: subcarrier assignment solved by the average capacity metric (AC-metric) combined with Hungarian algorithm and power allocation, which equals to a nonlinear programming solved by the gradient projection method (GPM). As for two-cell CR systems, we establish a noncooperative game, which performs uplink subcarrier assignment and power allocation among noncooperative CR cells with multiple CR users per cell. Since the optimization formulation for rate maximization of multiple users in each CR cell is an integer optimization problem, the multiple access channel (MAC) technique is applied to transform the integer optimization problem into a concave optimization problem. In practice, the channel state information (CSI) between CR users and licensed users cannot be perfectly known, and thus, an estimated CSI is considered by defining a prescribed outage probability of licensed systems.

The remainder of this chapter is organized as follows. Section 2 provides a systematic introduction of FBMC technique and makes a brief comparison with OFDM, GFDM, and UFMC. In Sections 3 and 4, two RA algorithms for single-cell and two-cell CR systems are presented to well evaluate the spectral efficiency of different multi-carrier modulations, respectively. Finally, conclusions are made in Section 5.

2. Multi-carrier modulation (MCM)

MCM is an efficient tool to overcome communication channel challenges by dividing the frequency spectrum into multiple subcarriers [4]. Compared with single carrier modulation (SCM), it is easier to tackle the frequency-selective multipath effect in future communication networks. In this section, the introductions of FBMC and other three MCM waveforms are given, in which the description of FBMC is the main concentration. At the end of this section, the properties of these four waveforms are discussed and some generalizations are summarized for a clear understanding of these waveforms.

2.1. Filter bank multi-carrier (FBMC)

The basic concept of FBMC modulation technology was first proposed by Chang and Saltherg in the middle of 1960s [13], but it was not paid much attention by scholars because of its complexity. In the 1990s of the last century, we are familiar with the discrete multi-tone (DMT) modulation and discrete wavelet multi-tone (DWMT) modulation, both of which are the special cases of FBMC modulation. In recent years, along with the increasing demands for high reliability and high-rate communication, while signal processing and electronic equipment have made significant progress, the realization of the principle structure of FBMC is relatively easy. As a result, it has aroused the interest of researchers once again.

Generally, FBMC mainly has three kinds of modulation modes: cosine modulated multi-tone (CMT), filtered multi-tone (FMT), and offset quadrature amplitude modulation-based OFDM (OQAM-OFDM). CMT uses the cosine modulated filter bank, which is the early FBMC modulation technology in the field of digital subscriber line (DSL). It has been applied in the

field of wireless applications recently. CMT not only has a high bandwidth efficiency but also has a blind detection capability [14]. Due to the reconstruction performance of CMT, the overlapping adjacent bands can be completely separated when the multiple neighbor frequency bands are transmitted at the same time. FMT is another form of FBMC modulation. Compared to CMT, the subcarriers of the FMT are not overlapping between the adjacent frequency bands. In order to avoid the overlapping of subcarriers, the guard band should be added between the subcarriers. Due to the use of the guard interval, the FMT system will waste some bandwidth. Therefore, the main difference between CMT and FMT lies in the use of special frequency bands. Recent FBMC technique is referred to as OQAM-OFDM. Compared to CMT and FMT, OQAM-OFDM has the highest stop-band attenuation for a fixed filter length and number of subcarriers [15].

According to the characteristics of OQAM, the transmission symbols of the OQAM-OFDM communication system are the real and imaginary parts of the complex quadrature amplitude modulation symbols [16], and the transmission time interval is half of the symbol period between the real and imaginary symbols. In addition, the reasonable design of the prototype filter can ensure that the frequency response of each subcarrier has a better roll-off characteristic, for reducing the spectrum leakage of subcarriers. Many scholars have been designing suitable filters for FBMC. The filter using the frequency sampling technique in Ref. [24] has been considered as the reference prototype filter of the European project PHYDYAS. Le Floch [25] gives an overview of the main features concerning isotropic orthogonal transform algorithm (IOTA). The authors in Ref. [20] formulate a direct optimization problem of the filter impulse response coefficients for the FBMC systems to minimize the stop-band energy and constrain the ISI/ICI. In Ref. [26], it is attempted to design the prototype filter by performing time-frequency analysis on the ambiguity function of isotropic Hermite pulses.

Besides the research of prototype filter, people have made plenty of contributions to improve the performance of FBMC structure. In Ref. [27], a novel architecture for MIMO transmission and reception of FBMC modulated signals under strong frequency selectivity channel is presented. An improved partial transmit sequence (PTS) scheme by employing multi-block joint optimization (MBJO) for the PAPR reduction of FBMC signals is proposed in Ref. [28]. In Ref. [29], a novel scattered pilot method for channel estimation in FBMC is proposed. In Ref. [30], the authors propose a low complexity frequency offset compensation method for FBMC in a context of frequency division multiple access (FDMA). In Ref. [22], a data-aided joint maximum likelihood (ML) estimator of carrier frequency offset (CFO) and channel impulse response for oversampled perfect reconstruction filter banks transceivers are proposed. And the spectral efficiency of FBMC-based CR networks is studied in Ref. [17]. In short, FBMC has made some achievements in various aspects.

To conclude, the above three FBMC techniques could all theoretically offer a significant bandwidth efficiency advantage over OFDM due to their special filter bank based structure and the elimination of cyclic prefix (CP). On the other hand, among different FBMC techniques, OQAM-OFDM is preferred to be a suitable choice for CR applications since FMT and CMT are originally introduced for DSL applications and will be impractical and hard to meet the CR

http://dx.doi.org/10.5772/66057

system requirements. In this chapter, unless otherwise stated, the FBMC refers to OQAM-OFDM.

2.2. Other multi-carrier waveforms

In order to reflect the spectral efficiency performance of FBMC in CR systems, we compare it with OFDM, GFDM, and UFMC. In the following, we first introduce the other three modulation waveforms, and then, the differences in the four MCM waveforms are summarized. Contrast to FBMC, OFDM has a lower computational complexity [31]. It also can be combined with other technologies easily, such as wavelet orthogonal frequency division multiplexing (WOFDM) and MIMO. However, it has serious out-of-band leakage and high peak-to-average power ratio (PAPR) [32]. Until now, the ways to reduce PAPR are still being researched.

In GFDM system, the use of root-raised cosine (RRC) pulse-shaping filter can greatly reduce the impact of radiation and enhance the system flexibility. In addition, GFDM uses less CP, which improves the spectral efficiency [33, 34]. Similar to FBMC, GFDM can well integrate the spectrum. According to the requirements of the different types of services and applications, GFDM can choose different pulse-shaping filters and insert different types of CP. The subcarriers of GFDM pass through the effective prototype filter to filter and circularly shift both in time and in frequency domain, which reduces the band leakage. However, to meet the requirements of the quality of wireless communication transmission, GFDM technology sacrifices the bit error rate (BER) and the ICI at the cost of eliminating the band radiation [35]. In recent years, the focus of the research on GFDM technology lies in how to improve the BER performance and reduce the computational complexity.

UFMC has the advantages of the FBMC system, and it can also support different types of business [36]. Compared to the prototype filters of FBMC, UFMC uses a shorter filter length, which can support the short burst asynchronous communication [37]. Furthermore, UFMC system has a low requirement about time-frequency calibration and non-orthogonality. However, similar to OFDM system, UFMC suffers the influence of both the Doppler effect and the crystal oscillators of transmitter and receiver, which can result in the CFO. A small CFO will also lead to a sharp decrease in UFMC system performance. Therefore, in order to effectively reduce the interference in UFMC system so that it can improve the transmission reliability and ensure the effectiveness of the signal, interference cancelation has become a hot spot in this field.

In conclusion, according to the previous introductions, we have listed the features about OFDM, FBMC, GFDM, and UFMC in **Table 1** [1–4, 37, 38], including the PAPR, the out of band, and the spectral efficiency we are concerned about. According to these characteristics, we can make a rough comparison of these four kinds of waveforms. And the superiority and inferiority of each waveform are also clearly presented. We can select different waveforms based on various application scenarios.

	OFDM	FBMC	GFDM	UFMC
PAPR	High	High	Low	Medium
Out of band	High	Low	Low	Low
Spectral efficiency	Medium	High	Medium	High
CP	Yes	No	Yes	No
Orthogonality	Yes	Yes	No	Yes
Synchronization requirement	High	Low	Medium	Low
Ease of integration with MIMO	Yes	No	Yes	Yes
Latency	Short	Long	Short	Short
Effect of frequency offset	Medium	Medium	Medium	Medium

Table 1. Comparison of the features among OFDM, FBMC, GFDM, and UFMC.

It is seen that these four modulation waveforms have their own drawbacks and superiorities. In addition, we have simulated the BER of these four waveforms, which is an important factor to measure the modulation waveforms [39]. The BER performance in different signal noise ratios (SNRs) is shown in **Figure 1**, where the parameters of these modulation waveforms are as follows: the number of subcarriers of FBMC is 128, and the prototype filter of FBMC is the PHYDYAS filter [40]; the number of subcarriers of OFDM is 128, and the prototype filter of

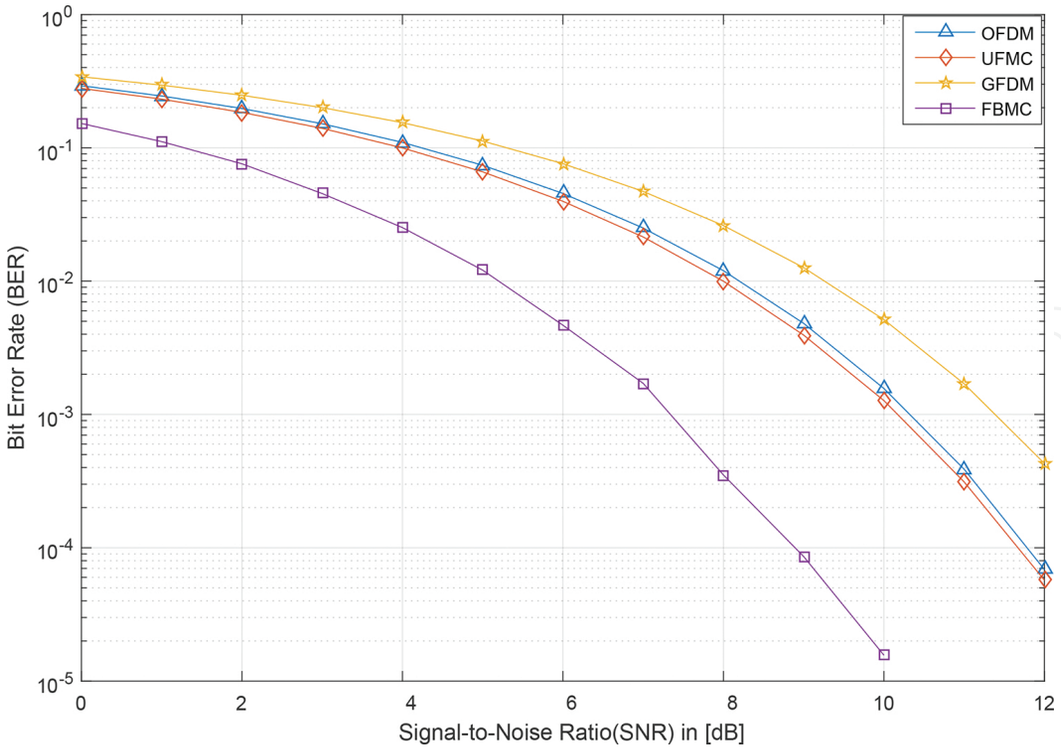

Figure 1. BER vs. SNR levels for FBMC-, OFDM-, GFDM-, and UFMC-based systems.

http://dx.doi.org/10.5772/66057

OFDM is the rectangle filter; the number of subcarriers of GFDM is 128, the number of sub-symbols of GFDM is 9 in each subcarrier, and the prototype filter of GFDM is the RRC filter with roll-off coefficient $\alpha = 0.5$; the number of sub-bands of UFMC is 10, the number of subcarriers of UFMC is 12 in each sub-band, and the prototype filter of UFMC is the Dolph-Chebyshev filter [36].

The prototype filter is a key element in the MCM schemes because all synthesis and analysis filters are frequency-shifted versions of the corresponding low-pass prototype filter frequency response. The principle how we select the prototype filter is that the most commonly used prototype filter is chosen in the research of different waveforms. For FBMC, we adopt the prototype filter used in PHYDYAS project [27–30], which can reduce the side-lobe of FBMC effectively. For OFDM, the rectangular filter is chosen as the prototype filter, which is one of the most popular prototype filters in the OFDM theory model. For GFDM, we use RRC filter which has a lower spectrum leakage in the frequency domain if the roll-off coefficient is larger. Normally, when the GFDM system is studied, the RRC filter [34, 35] is widely used as the prototype filter. For UFMC, we adopt Dolph-Chebyshev filter used in Ref. [36], which proposes the method for designing UFMC. Another important reason for the selection of these prototype filters is that they play their respective advantages in different modulation structures. For example, the use of RRC filter makes the GFDM flexible, which might be difficult to realize by other prototype filters.

It is noted from **Figure 1** that the BER of FBMC is the lowest than those of other waveforms in different SNRs, which means FBMC has the best BER performance than other three modulation waveforms. The BER performance of GFDM is the worst, while the BER performance of UFMC is better than that of OFDM.

In this chapter, the interferences of side-lobe radiation in these MCM modulations are the focus of consideration. **Figure 2** shows the frequency responses of prototype filters for FBMC, OFDM, GFDM, and UFMC. Although the energy is mainly located in the main lobe, it is intuitively clear that the four modulations have different side-lobe radiations. FBMC has the minimum out-of-band leakage, and the out-of-band leakage of OFDM is the largest, while the out-of-band leakage of GFDM is larger than that of UFMC, that is, the interference that depends on the out-of-band leakage among subcarriers of different modulations is not the same. The reason why they have different spectrum leakages, to a large extent, depends on the prototype filters they use. Hence, if we want to establish an interference model, it can be based on the side-lobe radiation, which is determined by the power spectral density (PSD) model of multi-carrier signals. According to the PSD-based approach in Ref. [41], the interference values of each modulation scheme can constitute an interference vector. This is an important measure to distinguish different waveforms in the following sections. The interference vectors of FBMC and OFDM are referred in Refs. [41, 42]. Assuming that a single complex symbol with power equals to "1," the element of vectors is the power of out-of-band radiation. The interference vectors of UFMC and GFDM are calculated with the same method in Refs. [41, 42], wherein interference less than 10^{-3} is ignored. Thus, the interference vectors are derived as

$$\begin{cases} V^{fbmc} = [6.38e^{-2}, 0, 0, 0, 0, 0, 0] \\ V^{ofdm} = [6.31e^{-2}, 1.07e^{-2}, 4.42e^{-3}, 2.52e^{-3}, 1.73e^{-3}, 1.31e^{-3}, 1.02e^{-3}] \\ V^{ufmc} = [12.27e^{-2}, 0, 0, 0, 0, 0, 0] \\ V^{gfdm} = [4.80e^{-2}, 4.18e^{-2}, 1.40e^{-3}, 0, 0, 0, 0] \end{cases}. \quad (1)$$

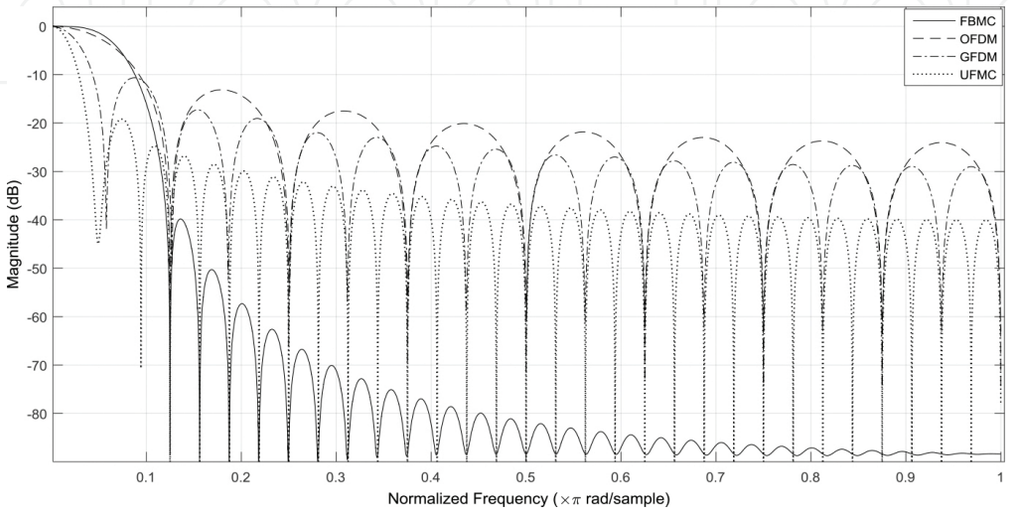

Figure 2. Frequency responses of prototype filters for FBMC, OFDM, GFDM, and UFMC.

This section compares the characteristics between FBMC and other three modulation schemes. The interference vectors are also given to quantify the out-of-band radiation, and they will be applied for the comparison of spectral efficiency among these four modulation waveforms in Sections 3 and 4.

3. Spectral efficiency comparison in single-cell systems

In this section, the RA of single CR cell with multiple CR users is designed to evaluate the spectral efficiency of FBMC and other three waveforms-based CR networks. The spectral efficiency is measured by the average capacity of available frequency bands, which is mainly determined by the MCM scheme and the RA strategy. Considering the low complexity, the proposed RA algorithm in the context of single CR cell is split into two sequential steps: subcarrier assignment and power allocation. In the following, the detailed statements including the system model and the RA algorithm are presented.

3.1. System model

In the context of CR systems, a group of SUs randomly distributed with an accessing point called secondary base station (SBS) constitutes a CR cell. As depicted in **Figure 3**, the uplink

http://dx.doi.org/10.5772/66057

scenario of CR systems incorporates a primary cell and a secondary cell with multiple PUs and SUs. Generally, due to the spectral leakage (indicated in **Figure 4**) and imperfect synchronization between SU and PU, the out-of-band radiation of a subcarrier will be regarded as interference. If the spectrum holes adjacent to the PUs are occupied by the SUs, the PUs may

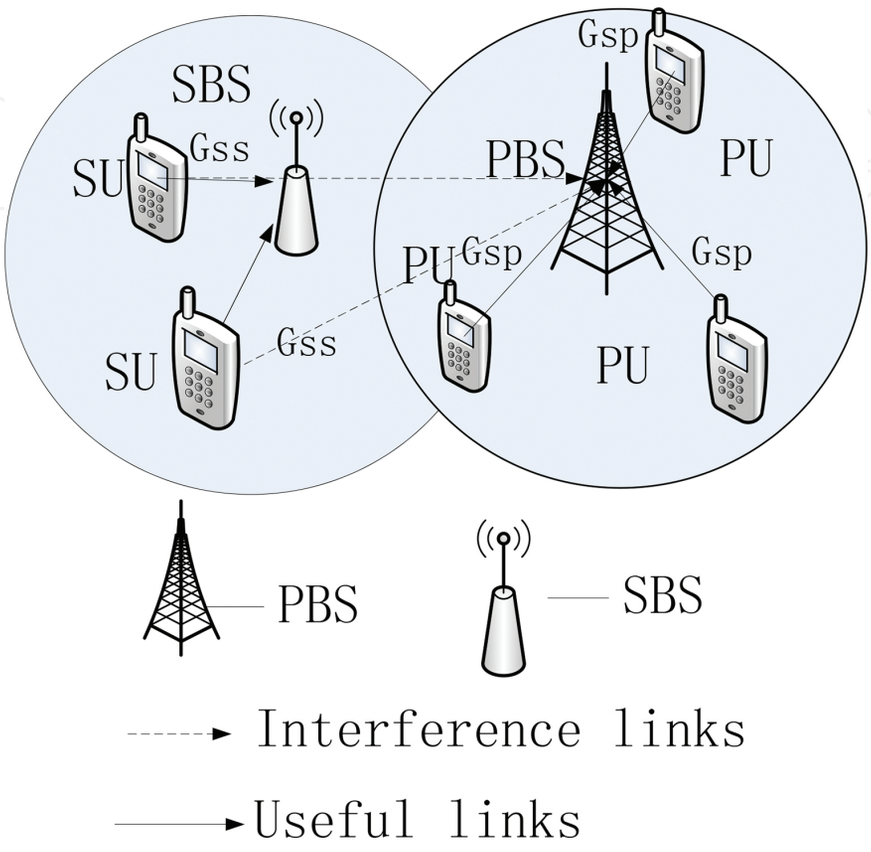

Figure 3. The system model of single CR cell including multiple users, the solid lines with arrow stand for the links producing the capacity, the dash lines with arrow stand for the interference links.

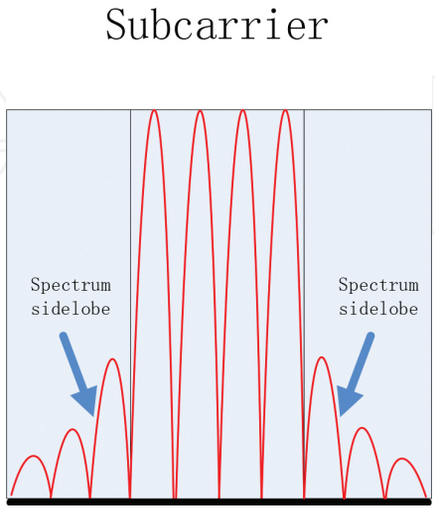

Figure 4. The neighbor frequency interference resulting from spectral leakage.

suffer from the intercell interference. For the guarantee of the quality of service (QoS) of PUs, the interference constraint must be considered to limit the interference from SUs. The distributions of PUs and the spectral holes are depicted in **Figure 5**. Assuming that the whole bandwidth is divided into 48 sub-bands, each sub-band includes $L = 18$ subcarriers. A spectrum hole may incorporate many sub-bands. As shown in **Figure 5**, the busy and idle sub-bands are represented by "1" and "0," respectively: "1" means the occupied frequency bands by PUs and "0" means the idle frequency bands to be dynamically accessed by SUs. Assuming that the SBS can perfectly sense the idle bands of the primary system and SUs in the CR cell are synchronized, the spectrum sensing error is not in consideration; therefore, the concentration is located in the RA scheme.

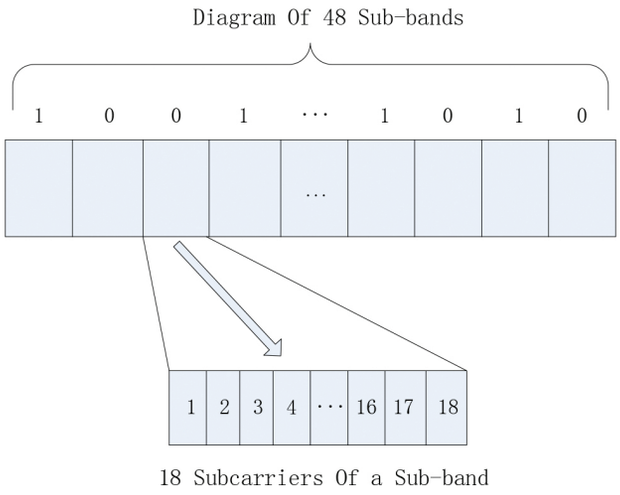

Figure 5. The diagram of idle and occupied frequency bands (a sub-band incorporates 18 subcarriers).

According to the above analysis, the CR cell wants to maximize its sum data rate by allocating power into the detected spectrum holes for its own users. Considering the information rate of user m on the f_{th} subcarrier of the k_{th} spectrum hole, the signal-to-interference-plus-noise ratio (SINR) with transmission power p_m^{kf} and transmission gain G_{ss}^{mkf} can be written as

$$\text{SINR} = \frac{p_m^{kf} G_{ss}^{mkf}}{\sigma^2 + I_f^k} \tag{2}$$

where σ^2 is the power of noise, and I_f^k is the interference power. Therefore, the information rate is obtained by the Shannon capacity theorem as

$$Rate = log_2\left[1 + \frac{p_m^{kf} G_{ss}^{mkf}}{\sigma^2 + I_f^k}\right]. \tag{3}$$

http://dx.doi.org/10.5772/66057

Noticed that whether the subcarrier is assigned to the user m or not, this can be represented through the subcarrier allocation indicator θ_m^{kf}. Assumed that there are M SUs, the number of spectrum holes is K, the number of subcarriers in the k_{th} spectrum hole is $F_{k'}$ the problem of maximizing the total information rate can be formulated as

$$Problem1: \max_{p}: C(p) = \sum_{m=1}^{M}\sum_{k=1}^{K}\sum_{f=1}^{F_k}\theta_m^{kf} log_2\left[1+\frac{p_m^{kf}G_{ss}^{mkf}}{\sigma^2+I_f^k}\right]$$

$$s.t.\begin{cases} \sum_{k=1}^{K}\sum_{f=1}^{F_k}\theta_m^{kf}\,p_m^{kf} \le P_{th}, & \forall m;\ (st1) \\ 0 \le p_m^{kf} \le P_{sub}, & \forall m,k,f;\ (st2) \\ \sum_{k=1}^{K}\sum_{h=1}^{H}\theta_m^{k_{l(r)}h}\,p_m^{k_{l(r)}h}G_{sp}^{mk_{l(r)}}\sum_{i=1}^{H-h+1}V_{H-i+1} \le I_{th}, & \forall k;\ (st3) \end{cases} \quad (4)$$

θ_m^{kf}	Binary variable $\theta_m^{kf} \in \{0,1\}$, $\theta_m^{kf}=1$ implies that the user m uses the f_{th} subcarrier in the k_{th} hole and $\theta_m^{kf}=0$ means the subcarrier is not accessed by the user
p_m^{kf}	User power on the f_{th} subcarrier in the k_{th} hole
G_{ss}^{mkf}	The channel gain from user m to SBS
σ^2	The noise power of each subcarrier
I_f^k	Interference from PU on the f_{th} subcarrier in the k_{th} hole
P_{th}	The user's sum power limitation
P_{sub}	Each subcarrier power limitation
$p_m^{k_{l(r)}n}$	The user power on the left (right) n_{th} subcarrier in the k_{th} hole
$G_{sp}^{mk_{l(r)}}$	The channel gain from SU to primary base station (PBS) on the left (right) primary subcarrier adjacent to the k_{th} hole
V_i	The i_{th} element of the interference vectors
V	Interference vector
H	The length of interference vector
L	The number of subcarriers in each sub-band
I_{th}	Interference threshold protecting the QoS of PUs

Table 2. Parameter definitions of CR system model.

The parameter definitions are shown in **Table 2**. While the first constraint $st1$ is to limit the sum maximum power of the SUs, the second constraint $st2$ specifies the range of each subcarrier power. The third constraint $st3$ indicates that the interference to PU should not exceed to the interference threshold I_{th}. In Eq. (4), the intercell interference from PU to SU I_f^k can be calculated as follows:

$$I_f^k = \begin{cases} \sum_{h=f}^{H} P_p^{k_l} G_{ps}^{k_l f} V_h, & f = 1,2,\ldots H \\ \sum_{h=F_{k-f+1}}^{H} P_p^{k_r} G_{ps}^{k_r f} V_h, & f = F_{k-f+1},\ldots F_k \\ 0, & \text{otherwise} \end{cases} \tag{5}$$

where $P_p^{k_{l(r)}}$ is the transmission power of PU located in the left (right) of the k_{th} spectrum hole, and $G_{ps}^{k_{l(r)}f}$ is the channel magnitude from PU located in the left (right) of the k_{th} spectrum hole to SBS on the f_{th} subcarrier of the k_{th} spectrum hole. The I_f^k can be measured during spectrum sensing by SBS without need to know this information.

The standards of CR systems are still being studied; to the best of our knowledge, the interference threshold I_{th} does not have a common definition in academic field. In order to make a trade-off between the QoS of PUs and the capacity of SUs, an appropriate interference threshold is needed. In this chapter, the interference threshold I_{th} is prescribed by the primary system through the capacity loss coefficient λ of PU. If there is no interference from SU, the capacity of PU in a sub-band is computed as follows: (Generally, the SNR in wireless communication systems is $-5 \sim 30$dB; here, we select the SNR = 10 in simulation test.)

$$C = log_2\left(1 + \frac{P_p G_{pp}}{L\sigma^2}\right) \tag{6}$$

$$\text{SNR} = \frac{P_p G_{pp}}{L\sigma^2} = 2^C - 1 \tag{7}$$

http://dx.doi.org/10.5772/66057

where P_p and G_{pp} are the power of PU and the channel gain from PU to primary base station (PBS), respectively. Considering the interference threshold I_{th}, the minimal capacity and the SINR of PU are

$$C_2 = log_2\left(1+\frac{P_p G_{pp}}{L\sigma^2 + I_{th}}\right) \tag{8}$$

$$\text{SINR} = \frac{P_p G_{pp}}{L\sigma^2 + I_{th}} = 2^{C_2} - 1. \tag{9}$$

Comparing Eqs. (7) and (9), we obtain

$$\frac{I_{th}}{L\sigma^2} = \frac{2^C - 1}{2^{C_2} - 1} - 1. \tag{10}$$

Defining the tolerable capacity loss coefficient λ of primary system, then we have

$$C_2 = (1-\lambda)C. \tag{11}$$

Substituting Eq. (11) into Eq. (10), I_{th} is fully determined by the value of C and the capacity loss coefficient λ

$$I_{th} = \left(\frac{2^C - 1}{2^{(1-\lambda)C} - 1} - 1\right) L\sigma^2. \tag{12}$$

Defining different values of λ, there are corresponding different levels of interference threshold. The larger the value of λ is, the more interference the primary system can tolerate.

Besides the interference threshold I_{th}, another considered parameter is the channel gain G_{sp}. In fact, perfect CSI in RA problem [43–45] cannot be obtained because of channel delays and

hardware limitation in channel estimation. In Section 3.2.3, we will describe the channel estimation of $G_{sp}^{mk_{l(r)}}$ in detail.

3.2. Resource allocation

The RA problem in communication systems generally needs to simultaneously solve two kinds of tasks: the channel assignment and the power allocation. Instead of pursuing an optimal solution, RA algorithms in many existing works search for a suboptimal solution which decomposes the RA problem into two steps: first assigning the subcarriers and then allocating the power [46, 47]. Generally, the solution of the suboptimal algorithm, which has low computational complexity, can be close to that of the optimal one. Therefore, the suboptimal idea is inherited, and an efficient suboptimal algorithm solving the optimization problem in Eq. (2) is presented as follows.

3.2.1. Subcarrier assignment

The first task of subcarrier assignment is the bandwidth allocation. From the view of fairness, the SU which exhibits the minimum average capacity always increases the number of its subcarriers until the total number of sub-bands assigned to SUs equals to the number of free sub-bands. This mechanism helps to promise that each SU can achieve the fairness. Assuming that F is the number of free sub-bands, the number of SUs is M ($F > M$), and N^i stands for the number of sub-bands assigned to the i_{th} user. Then, the number of sub-bands can be determined according to the steps below:

① First, suppose that each SU has the equal number of sub-bands, given as: $N^i = F/M,\ \forall\ i$ where x denotes the largest integer not exceeding x.

② Second, calculate the average capacity of each SU $C^i = N^i log_2\left(1 + \frac{\overline{G}_i \frac{P_{th}}{N^i}}{\sigma^2}\right)$. Find the SU with minimal capacity: $i' = \arg min_i(C^i)$. And then add the sub-band number of SU i', i.e., $N^{i'} = N^{i'} + 1$.

③ If all available sub-bands are allocated (which means $\sum_{i=1}^{M} N^i = F$), terminate. Else, repeat the step ②.

Next, the relevant subcarrier assignment is completed. In traditional multi-carrier systems, a good channel quality depends on its high SNR. The maximum SNR-metric is widely applied to assign the subcarriers to the user by the value of SNR "$\bar{P}G_{ss}/\sigma^2$" ($\bar{P}$ is the averaged power by dividing the total power budget on the number of the subcarriers), which only considers

http://dx.doi.org/10.5772/66057

the channel gain factor. Therefore, the SNR-metric is not accurate enough to assess the average capacity in CR systems.

In order to obtain the average capacity precisely, the average capacity metric (AC-metric) is applied to take more factors into account. The AC-metric is decided by the channel gain G_{ss}, the interference threshold I_{th}, the user power limitation P_{th}, and the channel gain G_{sp}. AC-metric makes a balance between all these influence factors. **Figure 6** shows four different styles of sub-bands in idle spectrum holes, and the average capacity of each style can be calculated by Eq. (12), where C1, C2, C3, and C4 stand for the average capacities of the four different sub-bands, respectively. H is the length of interference vectors, $SINR_h^{l(r)}$ is the SINR on the left (right) h_{th} subcarrier of one spectrum hole, $p_h^{l(r)}$ represents the power on the left (right) h_{th} subcarrier of one spectrum hole, $G_{ss}^{l(r)h}$ stands for the channel magnitude of SU to SBS on the left (right) h_{th} subcarrier.

Assuming that there are K^u SUs and K^c idle sub-bands, a $K^c \times K^c$ AC-matrix can be obtained using the bandwidth allocation method. Our task is how to optimally assign these K^c sub-bands to the K^u SUs, which equals to the search of the optimal matching of a bipartite graph, and the Hungarian algorithm [48] can efficiently solve this assignment problem. Therefore, the subcarrier assignment is implemented by means of AC-metric and the Hungarian algorithm.

$$\begin{cases} C1 = \dfrac{\sum_{h=1}^{H} log_2\left(1+SINR_h^l\right)+\sum_{h=1}^{H} log_2\left(1+SINR_h^r\right)+(18-2N)log_2\left(1+\dfrac{P_{th}-P_l-P_r}{(18-2H)\sigma^2}\right)}{18} \\ C2 = \dfrac{\sum_{h=1}^{H} log_2\left(1+SINR_h^l\right)+(18-H)log_2\left(1+\dfrac{P_{th}-P_l}{(18-H)\sigma^2}\right)}{18} \\ C3 = \dfrac{\sum_{h=1}^{H} log_2\left(1+SINR_h^r\right)+(18-H)log_2\left(1+\dfrac{P_{th}-P_r}{(18-H)\sigma^2}\right)}{18} \\ C4 = log_2\left(1+\dfrac{\bar{p}G_{ss}}{\sigma^2}\right) \\ SINR_h^l = \dfrac{p_h^l G_{ss}^{lh}}{\sigma^2+I_n^l} \quad SINR_h^r = \dfrac{p_h^r G_{ss}^{rh}}{\sigma^2+I_l^r} \\ p_h^l = \min\left\{\bar{P}, \dfrac{I_{th}}{LV_h G_{sp}^l}\right\}, p_h^r = \min\left\{\bar{P}, \dfrac{I_{th}}{LV_h G_{sp}^r}\right\} \end{cases} \tag{13}$$

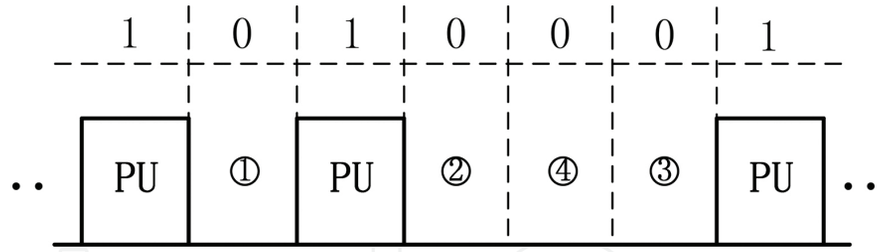

Figure 6. Four different types of sub-bands in available spectrum holes.

3.2.2. Power allocation

The subcarrier assignment has been discussed in Section 3.2.1. In this subsection, the focus is on the problem of power allocation. At the premise of knowing the result of the subcarrier assignment, the power allocation of multiuser system can be virtually regarded as a single-user system. Hence, the task becomes a nonlinear programming, which can be efficiently solved by some algorithms, such as the Lagrangian multiplier and the gradient projection method (GPM) [49]. Considering that the nonlinear programming has the expression as Eq. (14), the Lagrangian multiplier is computational complex if there are extensive multipliers. Instead, the GPM can be applied to obtain the optimal power allocation solution in Eq. (14) with a low computational complexity. The steps of GPM are summarized in **Table 3**.

$$\begin{aligned} &\textit{Objective function}: \ \max f(x) \\ &s.t. \begin{cases} Ax < b \ ; \\ Ex = e \ ; \end{cases} \end{aligned} \tag{14}$$

Steps	
Step 1:	Find the projection matrix $P = I - E^T(EE^T)^{-1}E$. E is the coefficient matrix of active constraints
Step 2:	Calculate the next iteration direction $d_{k+1} = P \times \nabla f(x_k)$,$\nabla f(x_k)$ is the gradient of current iteration point
Step 3:	If $\left\|\left\|d_k\right\|\right\| \leq \epsilon$ or iteration times equal to the predetermined threshold, quit the iteration. (ϵ is the threshold of norm)
Step 4:	Calculate the range of step size α_{max}. $c = b - Ax$, $f = Ad_k \alpha_i = \frac{c_i}{f_i}$ if $f_i > 0$, $\alpha_i = \infty$ if $f_i \leq 0$
Step 5:	Find the step size α by line search
Step 6:	Compute the next iteration point. $x_{k+1} = x_k + \alpha d_k$ and go to step 2
Step 7:	Quit the iteration

Table 3. Steps of the GPM algorithm to solve nonlinear programming with linear constraints.

http://dx.doi.org/10.5772/66057

3.2.3. Estimated channel state information (CSI)

Generally, it is not practical to assume that the perfect CSI in RA problem is available. Due to the channel delays and the inaccuracy of channel gain estimation, there is always an estimation error between estimated CSI and ideal CSI. Thus, the estimated CSI has a more practical significance in communication research than the ideal CSI.

Notice that in $Problem1$, the channel gains include the gain from SU to SBS $G_{ss'}$ the gain from SU to PBS $G_{sp'}$ and the gain from PU to SBS G_{ps}. Although there are multiple types of channel links, there is no need to estimate all kinds of links for channel estimation load. We concentrate on the capacity of secondary cell and control its interference to primary cell. It is reasonable to assume that the channel gain G_{sp} from SU to PBS is not obtained and needs to be estimated, while the other types of links are known by SBS. The interference constraint cannot be tackled without the necessary information of the channel gain G_{sp} from SU to PBS. Although we do not know the channel gain $G_{sp'}$ the path loss gain G_{pl} of the link from PBS to SU on the subcarriers used by the primary system can be computed, and through interpolation, the channel gain G_{sp} on free subcarriers can be acquired. If frequency division duplex is applied, the downlink channel gain is not equal to the uplink channel gain. In this case, the downlink channel gain can be used as a rough estimate of the uplink channel gain. In addition, to guarantee the QoS of primary systems, a channel gain margin G_m is added on the pathloss gain G_{pl}. Thus, the estimated channel gain $\overline{G_{sp}}$ can be computed by

$$\overline{G_{sp}} = \left(1 + G_m\right) G_{pl}. \tag{15}$$

The G_m is associated with the prescribed outage probability P_{out} tolerated by the primary sytem. Based on the implicit hypothesis that there is no difference between the downlink and the uplink path loss, the evaluation of $\overline{G_{sp}}$ only depends on the Rayleigh fading. When the actual channel gain G_{sp} is larger than the estimated channel gain $\overline{G_{sp'}}$ we define this case as the outage of primary system. The outage probability P_{out} can be represented as

$$P_{out} = P\left(G_{sp} > \overline{G_{sp}}\right) = P\left(H_{sp}^2 G_{pl} > \left(1 + G_m\right) G_{pl}\right) = P\left(H_{sp}^2 > \left(1 + G_m\right)\right) \tag{16}$$

where $G_{sp} = H_{sp}^2 G_{pl'}$ H_{sp} is the Rayleigh fading frequency response. Since H_{sp} ~ Rayleigh (μ), the H_{sp}^2 has a Gamma distribution with shape parameter $\alpha = 1$ and scale parameter $\beta = 2\mu^2$. The cumulative distribution function of H_{sp}^2 is the regularized Gamma function. Therefore, Eq. (16) can be further described as

$$1 - P_{out} = \frac{\gamma\left(\alpha, \frac{1+G_m}{\beta}\right)}{\Gamma(\alpha)} \tag{17}$$

where γ is the lower incomplete gamma function. Then, given a tolerant outage probability P_{out} of primary system, the channel gain margin G_m will be determined by Eq. (17)

$$G_m = 2\mu^2 log_e\left(\frac{1}{P_{out}}\right) - 1\,. \tag{18}$$

According to the path loss gain G_{pl} and the outage probability P_{out} in Eq. (15), the estimated channel gain can be obtained.

3.3. Numerical results

The spectral efficiency of FBMC and the other three modulation waveforms are evaluated by using the abovementioned RA algorithm. We analyze the channel capacity of these waveforms in single CR cell systems from four aspects: the distance D between SBS and PBS, the maximal power of SUs P_{th}, the capacity loss coefficient λ of PU, and the outage probability P_{out} of PU. The simulation parameters are shown in **Table 4**, and the simulation results are illustrated in **Figures 7–10**.

Parameters	Value	Unit
Total bandwidth	10	MHz
Center frequency	2.5	GHz
Number of subcarriers	1024	–
Number of subcarriers in each sub-band	18	–
Power limitation of each subcarrier	5	mW
Noise power of each subcarrier	−134.1	dBm
Channel delays	$10^{-9}[0, 110, 190, 410]$	s
Channel powers	$[0, -9.7, -19.2, -22.8]$	dB

Table 4. Simulation parameters of single CR cell systems.

http://dx.doi.org/10.5772/66057

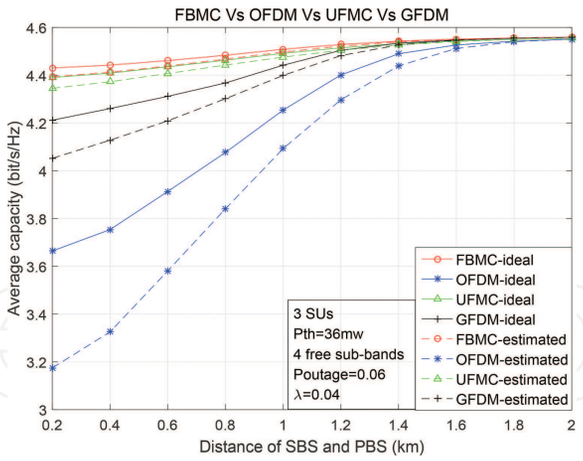

Figure 7. The relationship of capacity and distance between PBS and SBS.

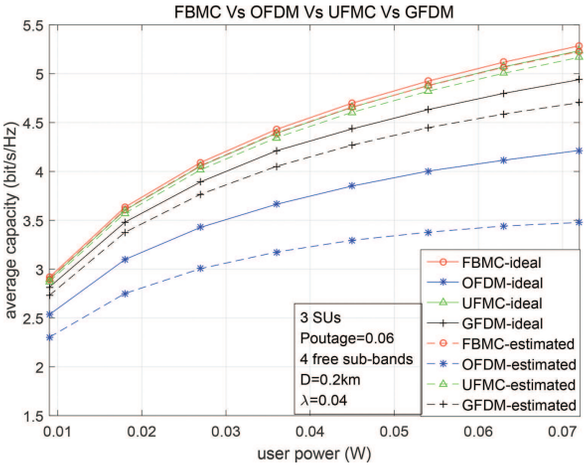

Figure 8. The relationship of capacity and the maximal power of SUs.

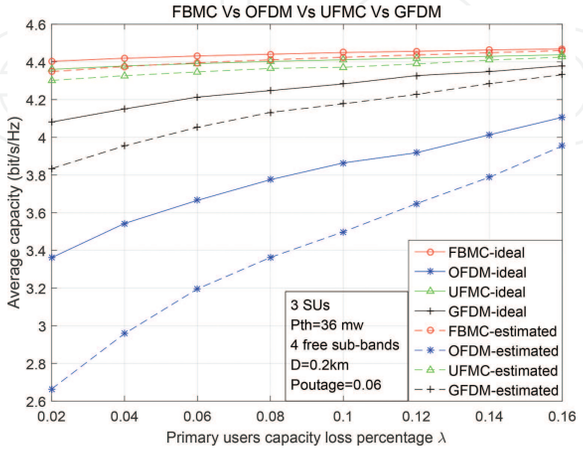

Figure 9. The relationship of capacity and interference threshold.

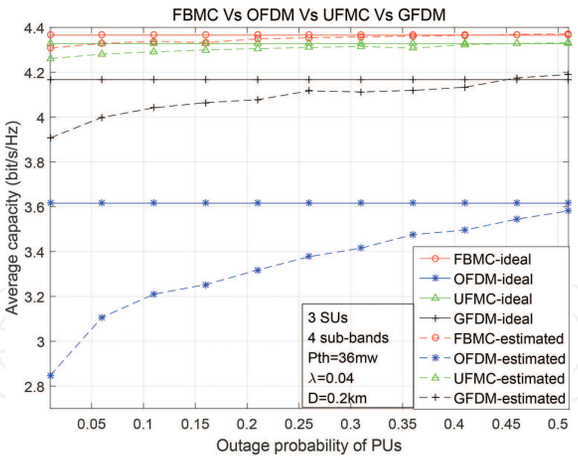

Figure 10. The relationship of capacity and the outage probability of PU.

The impact of the distance D between SBS and PBS on spectral efficiency is investigated in **Figure 7**. It can be seen that accompanied by the increase in the distance, the capacities of all waveforms arise and the curves tend to merge asymptotically. The increase in D reduces the mutual interference between the PU and the SU, which is the reason why the average capacity increases. The effect of the maximal power of SU P_{th} is assessed in **Figure 8**. We can obtain that the spectral efficiency of all waveforms increases with the augmentation of P_{th}. At the premise of satisfying the constraints, the larger power of SUs means that the more power is allocated to the spectrum holes, which results in the expansion of channel capacity.

Figures 9 and **10** evaluate the spectral efficiency from the perspective of PUs. **Figure 9** depicts the inherent interaction of average capacity and the capacity loss coefficient λ of PU. When less capacity loss is prescribed by PUs, which means a lower interference threshold and better protection for primary system, the achievable capacity degrades due to the more strict access control. **Figure 10** presents the relationship of spectral efficiency and the outage probability P_{out} of PU. Note that the average capacity of OFDM-based CR system with estimated CSI collapses when a low outage probability is prescribed, while other MCM-based CR systems are much less vulnerable to different outage probabilities.

3.4. Discussion of spectral efficiency in single-cell systems

From the above simulation results, some distinct conclusions can be drawn:

1. First, the results of **Figures 7–10** exhibit that the average capacity of FBMC outperforms those of other three waveforms. No matter what factor is considered, FBMC always has the highest spectral efficiency on the basis of capacity due to its slightest spectral leakage, UFMC comes second, GFDM takes the third place, and OFDM is the last. It implies that the less spectral leakage leads to the higher spectral efficiency in single CR cell systems.

2. Second, we can see that there is a channel capacity gap between the case of ideal CSI and the case of estimated CSI for the four MCM-based systems. It is easily found that the

http://dx.doi.org/10.5772/66057

spectral leakage property also plays an important role when the estimated CSI is considered. For the OFDM-based CR system, there is a large channel capacity gap between the case with ideal CSI and the case with an estimated CSI, while there is a slight capacity difference by applying the GFDM, UFMC, and especially the FBMC-based CR systems, which could be explained by the fact that when a low outage probability is required, more subcarriers adjacent to PU should be deactivated or underutilized for OFDM due to its significant spectral leakage, which accordingly decreases the channel capacity.

4. Spectral efficiency comparison in two-cell CR systems

In Section 3, the comparison of spectral efficiency in single CR cell is implemented easily by a two-step RA algorithm. However, in case of two CR cells, the situation becomes more complicated with a higher dimension of variables. Besides, different cells will compete for the common resource (assuming that the different CR cells will sense the same results of spectral holes). If the two CR cells use the same frequency bands to communicate, the co-channel interference will arise, which makes the RA problem difficult to tackle. In this section, a two-cell RA algorithm is proposed to evaluate the spectral efficiency of different MCM modulations. In the following, the system model is first introduced, and then, the RA optimization algorithm is elaborated. At last, simulation results will be given.

4.1. System model

In the scenario of two CR cells, as depicted in **Figure 11**, where the two CR cells with multiple users per cell are symmetrically distributed with the primary system, each CR cell is responsible for the allocation strategy of its users, and it introduces interference to primary system and another CR cell. Assuming that N denotes the number of cells, the number of users per cell is M. The aim is still to achieve the sum capacity of available frequency resource. Similar to the formulation of single-cell case, the expression of system model can be presented as

$$Problem\,2: \max_{p}: C(p) = \sum_{n=1}^{N}\sum_{m=1}^{M}\sum_{k=1}^{K}\sum_{f=1}^{F_k}\theta_{nm}^{kf} log_2\left[1+\frac{p_{nm}^{kf}G_{ss}^{nmkf}}{\sigma^2+I_{PS}^{nkf}+I_{SS}^{nkf}}\right]$$

$$s.t.\begin{cases}\sum_{k=1}^{K}\sum_{f=1}^{F_k}\theta_{nm}^{kf}p_{nm}^{kf}\le P_{th}, & \forall n,m;\,(st4)\\ 0\le p_{nm}^{kf}\le P_{sub}, & \forall n,m,k,f;\,(st5)\\ \sum_{k=1}^{K}\sum_{h=1}^{H}\theta_{nm}^{k_{l(r)}}p_{nm}^{k_{l(r)}h}G_{sp}^{nmk_{l(r)}}\sum_{i=1}^{H-h+1}V_{H-i+1}\le I_{th}, & \forall n,k;\,(st6)\end{cases} \tag{19}$$

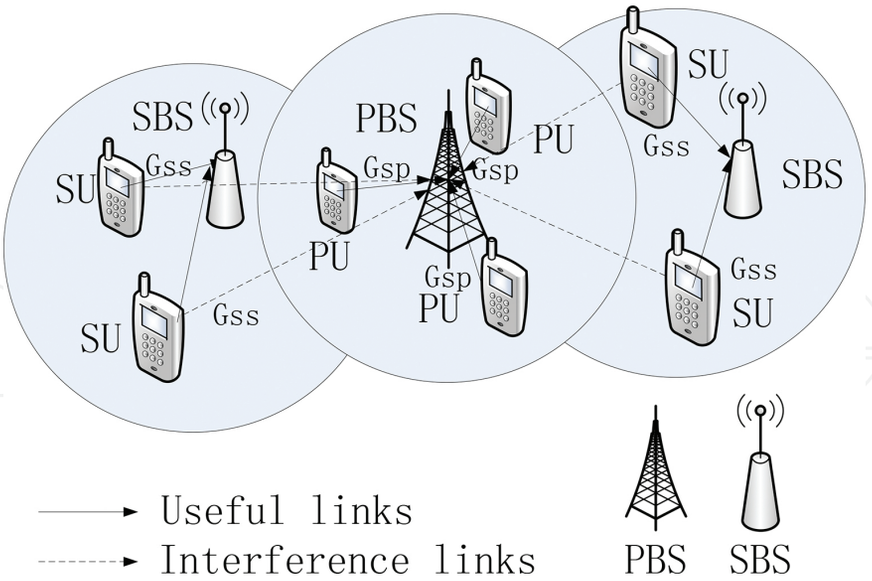

Figure 11. System model of two CR cells with multiple CR users per cell.

where the parameter definitions are the same with *Problem*1 in Eq. (4) and n stands for the n_{th} CR cell.

In Eq. (19), the mutual interference and the co-channel interference are computed as

$$I_{PS}^{nkf} = \begin{cases} \sum_{h=f}^{H} P_p^{nk_l} G_{ps}^{nk_l f} V_h, f = 1,2,\ldots H \\ \sum_{h=F_{k-f+1}}^{H} P_p^{nk_r} G_{ps}^{nk_r f} V_h, f = F_{k-f+1},\ldots F_k \\ 0, otherwise \end{cases} \tag{20}$$

$$I_{SS}^{nkf} = \sum_{n' \neq n}^{N} \sum_{m'=1}^{M} G_{SS}^{n'mkfn} p_{n'm}^{kf} . \tag{21}$$

To solve *Problem* 2 by centralized constrained optimization algorithms, all the channel gain information must be known. This causes large computational complexity and a huge amount of channel estimation overheads. Thus, a distributed RA algorithm is more appropriate than centralized optimization algorithms. Next, we will show our proposed algorithm for solving *Problem* 2 in a distributed manner by establishing a noncooperative game, where the convergence is desired.

http://dx.doi.org/10.5772/66057

4.2. Proposed algorithm for solving *Problem* 2

Distributed RA through a noncooperative game [50–53] is preferred where CR users in a single cell can make their own decision based on local information. It can significantly reduce the complexity and show an easier way in solving competition problem. Before the formulation of a noncooperative game, some mathematic preliminaries are given.

The structure of a noncooperative game A noncooperative game incorporates three elements: the players, the strategy space, and the utility function. A noncooperative game can be denoted by

$$g = \left\{ \boldsymbol{N}, \{p_n\}_{n \in \boldsymbol{N}}, \{u_n\}_{n \in \boldsymbol{N}} \right\} \tag{22}$$

N is the set of players in a game, $N = \{1, 2, 3, ..., N\}$. p_n is the strategy space of the n_{th} player. u_n is the utilization function of the n_{th} player. The competitive result of a noncooperative game is to obtain the Nash equilibrium (NE).

Definition of NE

A strategy profile p^* is NE if no unilateral deviation in strategy by any single player is profitable for that player, that is

$$u_n\left(p_n^*, p_{-n}^*\right) \geq u_n\left(p_n, p_{-n}^*\right) \ \forall n; \tag{23}$$

where p_n^* is the strategy of the n_{th} player on the NE point and p^*_{-n} is the strategy profile except for the n_{th} player on the NE point.

Existence of NE

Theorem: For a utility function $u_n(p_n, p_{-n})$ with a support domain which is a nonempty convex set, and u_n is continuous and quasiconvex or quasiconcave, at least a pure strategy NE point exists [50].

4.2.1. Formulation of the noncooperative game

Notice that the formulation in Eq. (19) is a mixed integer optimization problem, and the existence of the channel indicator θ_{nm}^{kf} does not satisfy the condition of converging to the NE. Therefore, our interest is casted on how to transform the foregoing problem Eq. (19) into a concave optimization problem. In Refs. [52, 54], the MAC technique [55–56] is advocated for the formulation of a nonlinear programming, which gives an idea of formulating a concave optimization problem.

Simple schemes like time division multiplexing access (TDMA) and FDMA are generally used in many practical situations. The MAC technique allowing more users to access the same channel assists to remove the indicator θ_{nm}^{kf}. In an MAC-based system, a channel via which two (or more) users send information to a common receiver, larger capacity region can be obtained than that achieved by TDMA or FDMA by using a common decoder for all the users of this system. Assuming that there are m senders denoted by $\{x_1, x_2, x_3, ..., x_m\}$ sending to a common single receiver with the power $\{p_1, p_2, p_3, ..., p_m\}$, $\{G_1, G_2, G_3, ..., G_m\}$ stands for the channel gains, and N_0 is the power of noise. MAC can get a large capacity region for these senders, and the capacity region can be calculated as

$$\sum_{i=1}^{m} R_i \le log_2\left(1 + \frac{p_1G_1 + p_2G_2 + p_3G_3 + \cdots + p_mG_m}{N_0}\right) \tag{24}$$

MAC can realize the channel assignment and eliminate the non-concave property which results from the channel indicator θ_{nm}^{kf}. Therefore, the task turns into being the power control on each subcarrier of users. With the help of MAC, the noncooperative game is formulated as

$$Problem\,3:\ max:\ u_n\left(p_n, p_{-n}\right) = \sum_{k=1}^{K}\sum_{f=1}^{F_k} log_2\left[1 + \frac{\sum_{m=1}^{M} p_{nm}^{kf} G_{ss}^{nmkf}}{\sigma^2 + I_{PS}^{nkf} + I_{SS}^{nkf}}\right]$$

$$s.t.\begin{cases} \sum_{k=1}^{K}\sum_{f=1}^{F_k} p_{nm}^{kf} \le P_{th}, & \forall n,m;(st7) \\ 0 \le p_{nm}^{kf} \le P_{sub}, & \forall n,m,k,f;(st8) \\ \sum_{k=1}^{K}\sum_{h=1}^{H} p_{nm}^{k_{l(r)}h} G_{sp}^{nmk_{l(r)}} \sum_{i=1}^{H-h+1} V_{H-i+1} \le I_{th}, & \forall n,k;(st9) \end{cases} \tag{25}$$

Notice that the objective function in *Problem* 3 is the summation of logarithmic functions, and the logarithmic function has the following style

$$f\left(x\right) = log_2\left(1 + a_1x_1 + a_2x_2 + a_3x_3 + \cdots + a_mx_m\right) \tag{26}$$

with parameters $[x_1, x_2, x_3, ..., x_m] \ge 0$. The summation of concave functions is still concave; therefore, if Eq. (26) is proved to be concave, then the objective function in Eq. (25) is also concave.

http://dx.doi.org/10.5772/66057

Proof: The Hessian matrix of $f(x)$ at point x is

$$\nabla^2 f(x) = -\frac{\left(1 + a_1x_1 + a_2x_2 + a_3x_3 + \cdots + a_mx_m\right)^{-2}}{log2} \times \begin{bmatrix} a_1^2 & a_1a_2 \cdots & a_1a_m \\ a_1a_2 & a_2^2 \cdots & a_2a_m \\ \cdots & \cdots \ddots & \cdots \\ a_1a_m & \cdots\cdots & a_m^2 \end{bmatrix} \\ = -\frac{\left(1 + a_1x_1 + a_2x_2 + a_3x_3 + \ldots + a_mx_m\right)^{-2}}{log2} \boldsymbol{aa^T} \tag{27}$$

where $\boldsymbol{a} = \left[\boldsymbol{a}_1\boldsymbol{a}_2\cdots\boldsymbol{a_m}\right]^{\boldsymbol{T}}$. For arbitrary row vector **P** with m elements, there are

$$\boldsymbol{P}\nabla^2 f(x)\boldsymbol{P}^T = -\frac{\left(1 + a_1x_1 + a_2x_2 + a_3x_3 + \ldots + a_mx_m\right)^{-2}}{log2} \times \left|\ \left|\mathbf{Pa}\right|\ \right|^2 \le 0 \tag{28}$$

Therefore, $f(x)$ in Eq. (26) is concave which also indicates that the objective function in *Problem* 3 is concave, which satisfies the existence condition of NE point, and thus, the convergence of *Problem* 3 is promised.

4.2.2. Determination of each cell's strategy

After the formulation of the noncooperative game, the next work is to determine the specific power allocation scheme. In the game theory-based algorithm, the power allocation scheme of each player is determined sequentially. It is observed that *Problem* 3 is a nonlinear programming with the same constraints as *Problem* 2. It has been shown that GPM is a useful tool to solve the nonlinear programming in the scenario of single CR cell. In order to solve *Problem* 3, GPM is still applied in the scenario of two CR cells. The steps of GPM have been presented in **Table 3**; for the sake of saving space, it is not restated. Readers are encouraged to review **Table 3** again if not familiar with GPM.

4.2.3. Estimated CSI of two CR cells

Based on the same assumption of single CR cell, each SBS has the perfect knowledge of its cell but does not have the CSI knowledge to PBS. Thus, the CSI in the link from SU to PBS is estimated. By means of estimating the channel gain G_{ps} in the inverse link from PBS to SU, the estimated CSI can be obtained with G_{ps} and G_m. It should be noticed that both of the two CR cells should conduct the CSI estimation. Since the specific process of channel state estimation has been stated in Section 3.2.3, there is no need for overmuch repeat.

4.3. Numerical results of two CR cells

With the same simulation parameters, the comparison of spectral efficiency between FBMC and other modulation waveforms in two CR cells is still assessed from the four aspects. According to the proposed RA algorithm of two CR cells, the simulation results are shown in **Figures 12–15**.

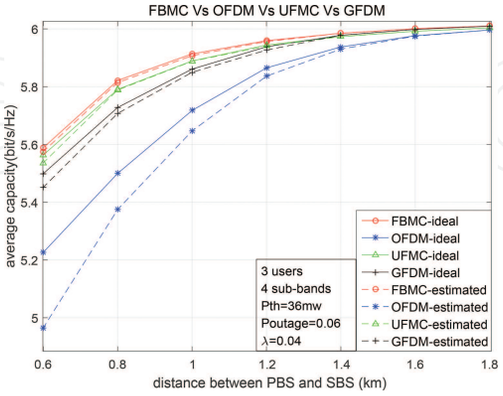

Figure 12. The relationship between distance and average capacity.

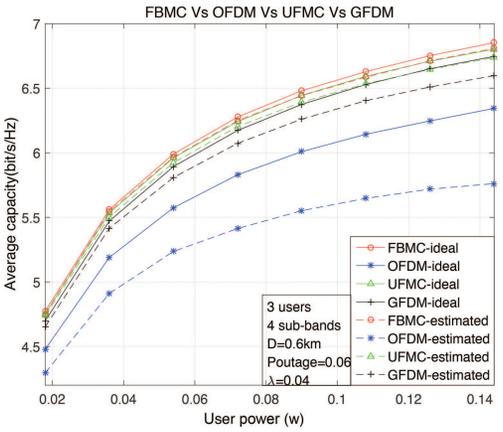

Figure 13. The relationship between interference threshold and average capacity.

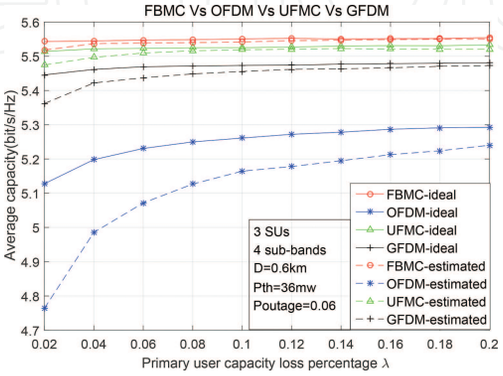

Figure 14. The relationship between user power and average capacity.

http://dx.doi.org/10.5772/66057

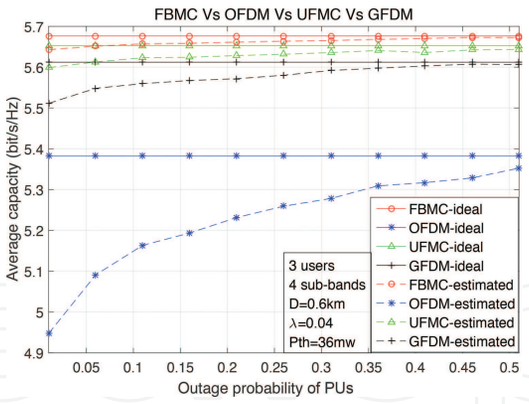

Figure 15. The relationship between outage probability and average capacity.

Figure 12 gives the impact of distance D between SBS and PBS in the context of two CR cells. We can find that the average capacity enlarges as the increase in distance similar to the case of single CR cell. However, compared to single CR cell, there is a clear difference that the span between the highest channel capacity and the lowest one of two CR cells is larger than that of single CR cell. This results from the co-channel interference; when the distance is small, there is an intense interference between the two CR cells in the common channel, which contributes to the dropping of capacity. When the distance becomes large gradually, both of the mutual interference and the co-channel interference wane with D, which explains why the curves merge. **Figure 13** assesses the spectral efficiency of two CR cells in terms of maximal user power. Although in the two CR cells, the user with larger power always can access by allocating more power to subcarriers and achieve a higher capacity, this explains the variation tendency of the capacity curves.

The relationship between capacity and the capacity loss coefficient λ of two CR cells is presented in **Figure 14**. Similar to the case of single CR cell, there is a slight capacity difference as the λ decreases for FBMC. If the primary system needs a strict protection for QoS, which means a low capacity loss coefficient λ, there is no doubt that FBMC is more able to meet the requirement. **Figure 15** shows the influence of average capacity and the outage probability of PU in the scenario of two CR cells. It is seen that FBMC has the best capacity performance with the slightest capacity difference between ideal and estimated CSIs if the same outage probability is considered. Although the performance curves of FBMC, UFMC, and GFDM are closer to each other than that in the case of single CR cell, the three waveforms show the dramatic difference from OFDM.

4.4. Discussions of spectral efficiency in two-cell systems

Based on the simulation results of single CR cell systems and two CR cells systems, the following discussions are presented.

1. Considering the case of two CR cells, we can conclude the same result as in single CR cell that FBMC shows the best spectral efficiency performance from any of the four aspects: the distance D between SBS and PBS, the interference threshold I_{th}, the maximal power

of SU P_{th}, and the outage probability P_{out} of PU. Moreover, compared to other waveforms, FBMC exhibits the best advantage when estimated CSI is considered.

2. The gaps of waveforms in two-cell CR system are smaller than those in the case of single cell. This can be explained as the existence of co-channel interference, which reduces the relative difference in total interference that a subcarrier can suffer. Compared to the single cell, the maximal average capacity of two cells is larger, which results from the application of the MAC technique that allows a large capacity region.
3. If more CR cells (>2) are considered, the co-channel interference will become larger and larger, and further narrow the difference in total interference. Therefore, it can be deduced that the spectral efficiency curves will be closer to each other.

Based on the above discussions, FBMC not only can achieve the largest channel capacity in the same constraints but also has the slightest capacity difference gap between perfect CSI and estimated CSI compared to other three MCM waveforms. As a consequence, FBMC technology providing the best system performance has been recommended in the future 5G communication networks.

5. Conclusion

In this chapter, the spectral efficiency comparison is conducted by analyzing the achievable channel capacity among four different multi-carrier modulations. Two RA algorithms with the practical consideration of estimated CSI are designed for evaluating and comparing the capacity performance. Simulation results show that in our scenarios, FBMC can offer the highest channel capacity and can achieve much more performance gain if rough estimated channel state information is considered. As a result, we conclude that the little spectral leakage of FBMC plays an essential role in achieving high spectral efficiency, and further verify that FBMC is a competitive candidate for 5G physical layer data communication.

Acknowledgements

This work was supported by the National Natural Science Foundation of China under Grant 61501335.

Author details

Haijian Zhang*, Hengwei Lv and Pandong Li

*Address all correspondence to: haijian.zhang@whu.edu.cn

School of Electronic Information, Wuhan University, Wuhan, China

References

[1] Banelli P, Buzzi S, Colavolpe G, Modenini A, Rusek F, Ugolini A. Modulation formats and waveforms for 5G networks: who will be the heir of OFDM? An overview of alternative modulation schemes for improved spectral efficiency. IEEE Signal Processing Magazine. 2014;31:80–93. doi:10.1109/MSP.2014.2337391

[2] Liu Q P, Yang Y N, Li W X. Application of OFDM technology in 4G mobile network. Applied Mechanics & Materials. 2014;631:851–855. doi:10.4028/www.scientific.net/AMM.631-632.851

[3] Tao Y, Liu L, Liu S, Zhang Z. A survey: several technologies of non-orthogonal transmission for 5G. China Communications. 2015;12:1–15. doi:10.1109/CC.2015.7315054

[4] Sahin A, Guvenc I, Arslan H. A survey on multicarrier communications: prototype filters, lattice structures, and implementation aspects. IEEE Communications Surveys & Tutorials. 2014;16(3):1312–1338. doi:10.1109/SURV.2013.121213.00263

[5] FP7 European Project 317669 METIS (Mobile and Wireless Communications Enablers for the Twenty-Twenty Information Society). 2012. Available from: https://www.metis2020.com/

[6] FP7 European Project 318555 5G NOW (5th Generation Non-Orthogonal Waveforms for Asynchronous Signalling). 2012. Available from: http://www.5gnow.eu/

[7] Lien S Y, Chen K C, Liang Y C, Lin Y. Cognitive radio resource management for future cellular networks. IEEE Wireless Communications. 2014;21:70–79. doi:10.1109/MWC.2014.6757899

[8] Sharma S K, Bogale T E, Chatzinotas S, Ottersten B, Le L B, Wang X. Cognitive radio techniques under practical imperfections: a survey. IEEE Communications Surveys & Tutorials. 2015;17:1858–1884. doi:10.1109/COMST.2015.2452414

[9] Zhang H J, Le Ruyet D, Roviras D, Sun H. Polyphase filter bank based multi-band spectrum sensing in cognitive radio systems. International Journal of Communication Systems. 2014;29:1844–1862. doi:10.1002/dac.2798

[10] Zhang L, Xiao P, Zafar A, Quddus A. ul Tafazolli R. FBMC System: an insight into doubly dispersive channel impact. IEEE Transactions on Vehicular Technology. doi:10.1109/TVT.2016.2602096

[11] Gregoratti D, Mestre X. Uplink FBMC/OQAM-based multiple access channel: distortion analysis under strong frequency selectivity. IEEE Transactions on Signal Processing. 2016;64:4260–4272. doi:10.1109/TSP.2016. 2566601

[12] Savaux V, Bader F, Palicot J. OFDM/OQAM blind equalization using CNA approach. IEEE Transactions on Signal Processing. 2016;64:2324–2333. doi:10.1109/TSP.2016.2519000

[13] Vaidyanathan P P. Multirate digital filters, filter banks, polyphase networks, and applications: a tutorial. Proceedings of the IEEE. 1990;78:56–93. doi:10.1109/5.52200

[14] Farhang-Boroujeny B. Multicarrier modulation with blind detection capability using cosine modulated filter banks. IEEE Transactions on Communications. 2003;51:2057–2070. doi:10.1109/TCOMM.2003.820753

[15] Amini P, Kempter R, Djoko-Kouam M. A comparison of alternative filterbank multicarrier methods for cognitive radio systems. Proceeding of the SDR Technical Conference and Product Exposition. 2006:1–6.

[16] Aminjavaheri A, Farhang A, Rezazadehreyhani A, Farhangboroujeny B. Filter bank multicarrier modulation: a waveform candidate for 5G and beyond. Advances in Electrical Engineering. 2014;2014:1–26. doi:10.1155/2014/482805

[17] Zhang H, Le Ruyet D, Terre M. Spectral efficiency comparison between OFDM/OQAM- and OFDM-based CR networks. Wireless Communications & Mobile Computing. 2009;9:1487–1501. doi:10.1002/wcm.704

[18] Kang A S, Vig R. Computational complexity analysis of FBMC-OQAM under different strategic conditions. Recent Advances Engineering and Computational Sciences (RAECS). 2014:1–6.

[19] Renfors M, Yli-Kaakinen J, Harris F J. Analysis and design of efficient and flexible fast-convolution based multirate filter banks. IEEE Transactions on Signal Processing. 2014;62:3768–3783. doi:10.1109/TSP.2014.2330331

[20] Chen D, Qu D, Jiang T, He Y. Prototype filter optimization to minimize stopband energy with NPR constraint for filter bank multicarrier modulation systems. IEEE Transactions on Signal Processing. 2013;61:159–169. doi:10.1109/TSP.2012.2222397

[21] Wu Y, Chen D, Jiang T. Efficient branch and bound algorithms for prototype filter optimization in OQAM-OFDM systems. International Journal of Communication Systems. 2015. doi:10.1002/dac.3031

[22] Rahimi S, Champagne B. Joint channel and frequency offset estimation for oversampled perfect reconstruction filter bank transceivers. IEEE Transactions on Communications. 2014;62:2009–2021. doi:10.1109/TCOMM.2014.2318717

[23] Caus M, Pérez-Neira A I. Multi-stream transmission for highly frequency selective channels in MIMO-FBMC/OQAM systems. IEEE Transactions on Signal Processing. 2014;62:786–796. doi:10.1109/TSP.2013.2293973

[24] Bellanger M G. Specification and design of a prototype filter for filter bank based multicarrier transmission. In Proceedings ICASSP, IEEE International Conference on Acoustics, Speech and Signal Processing; Salt Lake City, UT. 2001, pp. 2417–2420.

[25] Floch B L, Alard M, Berrou C. Coded orthogonal frequency division multiplex. Proceedings of the IEEE. 1995;83:982–996. doi:10.1109/5.387096

[26] Prakash J A, Reddy G R. Efficient prototype filter design for filter bank multicarrier (FBMC) system based on ambiguity function analysis of hermite polynomials. In International Multi-Conference on Automation, Computing, Communication, Control and Compressed Sensing, IEEE; Kottayam. 2013, pp. 580–585.

[27] Mestre X, Gregoratti D. Parallelized structures for MIMO FBMC under strong channel frequency selectivity. IEEE Transactions on Signal Processing. 2016;64:1200–1215. doi:10.1109/TSP.2015.2493988

[28] Qu D, Lu S, Jiang T. Multi-block joint optimization for the peak-to-average power ratio reduction of FBMC-OQAM signals. IEEE Transactions on Signal Processing. 2013;61:1605–1613. doi:10.1109/TSP.2013.2239991

[29] Cui W, Qu D, Jiang T, Farhang-Boroujeny B. Coded auxiliary pilots for channel estimation in FBMC-OQAM systems. IEEE Transactions on Vehicular Technology. 2016;65:2936–2946. doi:10.1109/TVT.2015.2448659

[30] Doré J B, Cassiau N, Ktenas D. Low complexity frequency domain carrier frequency offset compensation for uplink multiuser FBMC receiver. In European Conference on Networks and Communications; Bologna. 2014, pp. 1–5.

[31] Agnès N, Dooguy K A, Mohamed F S, Samuel O. Performance of a broadband multiple access system by spreading of OFDM symbols in a multipath channel. In 2015 World Congress on Information Technology and Computer Applications Congress (WCIT-CA); Hammamet. 2015, pp. 1–8.

[32] Hung Y C, Tsai S H L. PAPR analysis and mitigation algorithms for beamforming MIMO OFDM systems. IEEE Transactions on Wireless Communications. 2014;13:2588–2600. doi:10.1109/TWC.2014.031914.130347

[33] Fettweis G, Krondorf M, Bittner S. GFDM – generalized frequency division multiplexing. In IEEE 69th Vehicular Technology Conference (VTC Spring); Barcelona. 2009, pp. 1–4.

[34] Michailow N, et al. Generalized frequency division multiplexing for 5th generation cellular networks. IEEE Transactions on Communications. 2014;62:3045–3061. doi: 10.1109/TCOMM.2014.2345566

[35] Sendrei L, Marchevský S, Michailow N, Fettweis G. Iterative receiver for clipped GFDM signals. In Radioelektronika (RADIOELEKTRONIKA), 2014 24th International Conference; Bratislava. 2014, pp. 1–4.

[36] Vakilian V, Wild T, Schaich F, ten Brink S, Frigon J F. Universal-filtered multi-carrier technique for wireless systems beyond LTE. In 2013 IEEE Globecom Workshops (GC Wkshps); Atlanta, GA. 2013, pp. 223–228.

[37] Schaich F, Wild T, Chen Y. Waveform contenders for 5G – suitability for short packet and low latency transmissions. In 2014 IEEE 79th Vehicular Technology Conference (VTC Spring); Seoul. 2014, pp. 1–5.

[38] Long F. Signal processing techniques for 5G: an overview. ZTE Communications. 2015;2015:20–27. doi:10.3969/j.issn.1673-5188.2015.01.003

[39] Medjahdi Y, Terre M, Le Ruyet D, Roviras D, Dziri A. Performance analysis in the downlink of asynchronous OFDM/FBMC based multi-cellular networks. IEEE Transactions on Wireless Communications. 2011;10:2630–2639. doi:10.1109/TWC.2011.061311.101112

[40] FP7 European Project 211887 PHYDYAS, 2010 (PHYsical layer for DYnamic AccesS and cognitive radio). Available from: http://www.ict-phydyas.org

[41] Medjahdi Y, Terré M, Le Ruyet D, Roviras D. On the accuracy of PSD-based interference modeling of asynchronous OFDM/FBMC in spectrum coexistence context. In 2014 11th International Symposium on Wireless Communications Systems (ISWCS); Barcelona. 2014, pp. 638–642.

[42] Medjahdi Y, Terré M, Le Ruyet D, Roviras D. Interference tables: a useful model for interference analysis in asynchronous multicarrier transmission. EURASIP Journal on Advances in Signal Processing. 2014;2014:1–17. doi:10.1186/1687-6180-2014-54

[43] Wang X, Zhu P, Zheng F C, Meng C, You X. Energy-efficient resource allocation in multi-cell OFDMA systems with imperfect CSI. In 2015 IEEE 82nd Vehicular Technology Conference (VTC Fall); Boston, MA. 2015, pp. 1–5.

[44] Zhang Y Y, Wang Z W, Liu L H. Adaptive multi-user uplink resource allocation with imperfect CSI. In 11th International Conference on Wireless Communications, Networking and Mobile Computing (WiCOM 2015); Shanghai. 2015, pp. 1–5.

[45] Van Hecke J, Del Fiorentino P, Giannetti F, Lottici V, Vandendorpe L, Moeneclaey M. Resource allocation for multicarrier cooperative cognitive radio networks with imperfect channel state information. In 2014 IEEE 25th Annual International Symposium on Personal, Indoor, and Mobile Radio Communication (PIMRC); Washington, DC. 2014, pp. 653–658.

[46] Zhang H J, Le Ruyet D, Roviras D, Sun H. Spectral efficiency comparison of OFDM/FBMC for uplink cognitive radio networks. Eurasip Journal on Applied Signal Processing. 2010;2010:1–14. doi:10.1155/2010/621808

[47] Zhang H J, Le Ruyet D, Roviras D, Sun H. Capacity analysis of OFDM / FBMC based cognitive radio networks with estimated CSI. In 2010 Proceedings of the Fifth Interna-

tional Conference on Cognitive Radio Oriented Wireless Networks and Communications; Cannes. 2010, pp. 1–5.

[48] Kuhn H W. The Hungarian method for the assignment problem. Naval Research Logistics. 2005;52:7–21. doi:10.1002/nav.20053

[49] Barzaraa M S. Nonlinear Programming: Theory and Algorithms, 2nd ed. Hoboken, NJ: Wiley. 1993.

[50] Fudenberg D, Tirole J. Game Theory. Cambridge, MA: MIT Press. 1991.

[51] Wang B, Wu Y, Liu K J R. Game theory for cognitive radio networks: an overview. Computer Networks. 2010;54:2537–2561. doi:10.1016/j.comnet.2010.04.004

[52] Zhang H J, Le Ruyet D, Roviras D, Sun H. Noncooperative multicell resource allocation of FBMC-based cognitive radio systems. IEEE Transactions on Vehicular Technology. 2012;61:799–781. doi:10.1109/TVT.201 1.2180743

[53] Huang J, Sun Y, Chen Q. GALLERY: a game-theoretic resource allocation scheme for multicell device-to-device communications underlaying cellular networks. IEEE Internet of Things Journal. 2015;2:504–514. doi:10.1109/JIOT.2015.2419632

[54] Zhang H J. Filter bank based multi-carrier (FBMC) modulation for cognitive radio. Doctor Thesis, Conservatoire National des Arts et Metiers and Wuhan University. 2011.

[55] El Gamal A, Kim Y H. Network Information Theory. Cambridge, UK: Cambridge University Press. 2012.

[56] Mamandipoor B, Moshksar K, Khandani A K. Capacity-achieving distributions in Gaussian multiple access channel with peak power constraints. IEEE Transactions on Information Theory. 2014;60:6080–6092. doi:10.1109/TIT.2014.2342218

IntechOpen